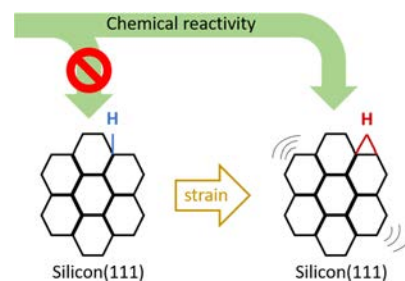


Strain Activation of Surface Chemistry on H-Terminated Si(111)

Tahereh Mohammadi Hafshejani, Jonas Wohlgemuth, and Peter Thissen*

ABSTRACT: Manipulation of the chemical and electronic properties of materials by strain is a widely accepted phenomenon. However, the impact of strain on microscopic aspects such as chemical reactivity is not clearly understood at the bond level. Here, we investigated the effect of strain on surface reactivity of H-Si(111). Analysis of FTIR data revealed that a decrease in stretching Si-H band's intensity and fluctuations in intensity of the bending Si-H mode, which are in relation to the appearance of a new peak, are correlated with each other. The underlying reason for the new peak is the formation of a three center bond as a result of diffusion of a hydrogen atom from the Si-H site. Our findings show that both the back bonds and the up bonds are easily oxidized due to the strain effect. In particular, the significant point is direct formation of Si-OH without any energy barrier. As strain is applied to the samples, the findings indicate that different oxidation pathways predominate.



1. INTRODUCTION

Sensitivity of the bare surface dangling bonds to any component of the environment makes the passivation of silicon surfaces an important issue in the area of semiconductor technology.¹⁻⁴ To be notably concerned is the stability of the hydrogen terminated surface in the clean room atmosphere of a production line.⁵⁻⁷ In addition, due to down scaling, the quality of the gate oxides is determined by the quality of the structural transition layer.⁸⁻¹⁰ Therefore, despite investigations on Si oxidation for many years, there is huge interest in the formation dynamics of Si/SiO₂ interfaces. Standard spectroscopic and microscopic structural analysis methods have been used in order to obtain a wide variety of information on oxidation kinetics. For example, spectroscopic ellipsometry provides data about growth rates.¹¹ Using the scanning tunneling microscopy and atomic force microscopy, the role of surface morphology during the oxidation was studied.^{12,13} Meanwhile, significant efforts were made for manipulation of Si oxidation kinetics. Considering that tensile stress elevates the overall rate of thermally grown oxides, manufacturing of Si based devices has been performed by uni- and biaxial strains.¹⁴ The effect of stress on a chemical reaction was revealed using the obtained data from the second harmonic generation (SHG).¹⁵ It was found that the reactivity of strained bonds relative to unstrained bonds at the same interface was increased by macroscopic tensile strain. Moreover, Daum et al. reported a suboxide form during oxidation by measurement of evolution of resonance in the SHG spectra of (111) oriented surfaces.¹⁶

Such findings provide enough evidence to manipulate in plane surface chemistry and for growing structures with interfaces designed at the bond level. Hence, there is a need to conduct a study on the strain effect on oxidation kinetics. So far, basic aspects of the initial stages of oxidation of unstrained

hydrogen terminated Si(111) (H-Si(111)) surfaces have been elucidated.^{6,15,17,18} Estimation of the rate of the surface oxidation process, which is especially sensitive to oxygen incorporations, was done by using the Si-H stretching mode as a probe.^{17,18} Chabal et al. found that a non integer order of 1.5 in the Si-H consumption rate is an indicator of a multistep mechanism of oxidation.¹⁷ In another study by Federico et al., they concluded that perfect hydrogenated Si(111) is unreactive toward H₂O vapor and O₂ at room temperature according to density functional theory (DFT).⁵ However, O₂, but not H₂O, reacts with silyl groups on a partially hydrogenated surface exposing silicon dangling bonds.

Strain is widely used to control chemical and electronic features of materials. However, it is not yet clear how strain affects the chemical reactivity at the bond level. Different issues remain elusive such as the rate of reactivity of the Si-H group by strain, change in the nature of intermediates, and the number of elementary reaction steps by strain. In the present study, the focus was on the initial step of oxidation via monitoring the Si-H stretch vibration on flat H-Si(111). Due to simplicity, H-Si(111) surfaces have been used leading to atomically smooth terraces with a homogenous array of identical Si-H bonds oriented normal to the surfaces.^{6,19} Second, water plays a prominent role. Most of the inorganic materials adsorb water in ambient air. Biology, materials science, and tribology are all influenced by adsorbed water.²⁰⁻²² The unique characteristics of water in the liquid

state originate from its large dipole moment, high polarizability, and capability for hydrogen bonding.^{23,24} Therefore, in this study, we confirmed the strain effect (at the atomic scale) on surface reactivity of the H-Si(111) surface both experimentally and theoretically.

2. METHODS

2.1. Sample Preparation. Pieces of p type (CZ, resistivity of 0.1–1 Ω cm) Si(111) wafers, polished on both sides, were prepared in 10 mm \times 30 mm \times 0.5 mm dimensions for mechanical measurements. In order to eliminate organic contaminations, samples were degreased in acetone, followed by a cleaning procedure by 30 min exposure to an 80 $^{\circ}$ C solution of 3:1 H₂SO₄ (96%):H₂O₂ (30%) (piranha solution). Hydrogen termination was performed on the samples in the order of a 30 s dip in 10–20% HF (aq), a 2.5 min dip in 40% NH₄F (aq), and a final rinse in H₂O for 10 s.

2.2. Straining the Samples and IR Measurement. Applying strain and IR measurement were done inside a N₂ purged glovebox with a mechanical machine illustrated in Figure 1.

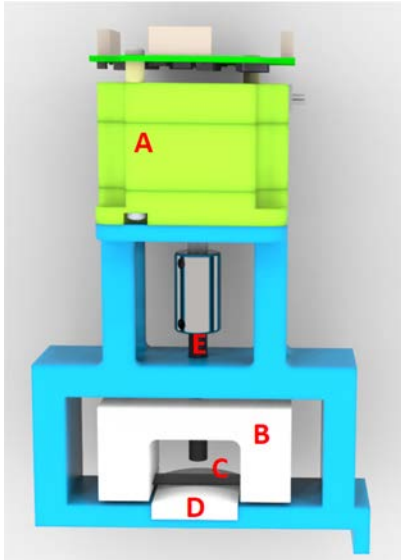


Figure 1. Schematic illustration of the proposed instrument, including: stepper motor (A), adjustable sample holder (B), sample (C), fixed curved metal piece (D), and spindle (E).

The adjustable holder (Figure 1B) is a part of the machine that moves toward the fixed curved metal piece at the bottom (Figure 1D). The sample (Figure 1C) is placed inside the slot of the sample holder. An open circuit connects the adjustable sample holder and the curved metal piece. When the sample and curved metal piece are in touch for the first time, the zero position is defined upon closing the circuit. The adjustable sample holder goes down 0.75 mm when a full rotation of the stepper motor is implemented, which in this motor equals 51,200 steps. To strain the sample at different values (0.006–1.0%), the sample is placed inside the sample holder, and the zero position is defined. In a program written in LabVIEW, the number of steps is set, which results in the downward movement of the spindle.

This creates a curvature on the sample, which is calculated as follows

$$\rho = \frac{x^2}{8d} \quad (1)$$

where x indicates the sample length (mm) and d depicts deflection (mm) in each position and ρ denotes the radius of curvature in each position (mm).

After the bending time has passed, the curvature is removed by entering a negative value for the number of steps (e.g., –1000) that correspond to the spindle's upward movement. The sample is removed from the sample holder and prepared for the following procedure.

At the end of each step, force and strain values on each deflection are calculated using the following equations

$$F = \frac{Ebh^3}{\rho 6x} \quad (2)$$

$$\epsilon = \frac{6Fxd}{Ebh^3} \quad (3)$$

where F represents the applied force (GPa mm²), x indicates the sample length (mm), d represents deflection (mm), E represents Young's modulus of Si (165 = GPa),²⁵ and ϵ represents the strain. b and h are the width and thickness of the sample, respectively. The procedures to obtain the proposed equations were thoroughly outlined in our previous article.²⁶ The applied values of deflection, strain, and force to get the strain in the range of 0.006–1% are presented in Table 1.

Table 1. Calculated Values of Deflection, Force, and Strain Corresponding to the Number of Steps

number of steps	deflection/ μ m	force/GPa mm ²	strain/%
400	5.8	4.475×10^{-24}	0.006
5000	73	5.594×10^{-23}	0.1
8400	123	9.399×10^{-23}	0.3
10800	158	1.208×10^{-22}	0.5
15400	225	1.723×10^{-22}	1.0

This experiment is divided into three steps: (I) investigation of the strain effect on the microstructure of H-Si(111), (II) investigation of surface reactivity of unstrained hydrogen terminated samples toward liquid water, and (III) the study of the reactivity of strained hydrogen terminated silicon (ϵ H-Si(111)) toward liquid water. Before each experiment, the silicon wafer (Si(111)) is cleaned with piranha solution and brought into a N₂ purged glovebox. The IR spectrum of the sample after the cleaning is obtained. Spectra with a nominal 4 cm⁻¹ resolutions were recorded (spectra from 400 to 4000 cm⁻¹, transmission mode) using a Fourier transform infrared spectrometer (VERTEX 70In). A room temperature pyroelectric detector (DTGS) was used for data collection. Furthermore, following the preparation of H-Si(111), all experiments (mechanical testing and IR measurement) on samples are carried out inside a glovebox.

For stage (I), after preparation of H-Si(111), the IR spectrum of the sample is measured. The side of the sample that has been exposed to the IR beam is marked. After the IR measurement, the sample is placed inside the sample holder (the marked side top). The zero position is defined and the number of steps is set 400 steps. The spindle turns and the sample holder moves down 5.8 μ m and the sample is kept under stress for 10 min. Subsequently, the curvature is removed, the sample is taken out, and the second IR spectrum

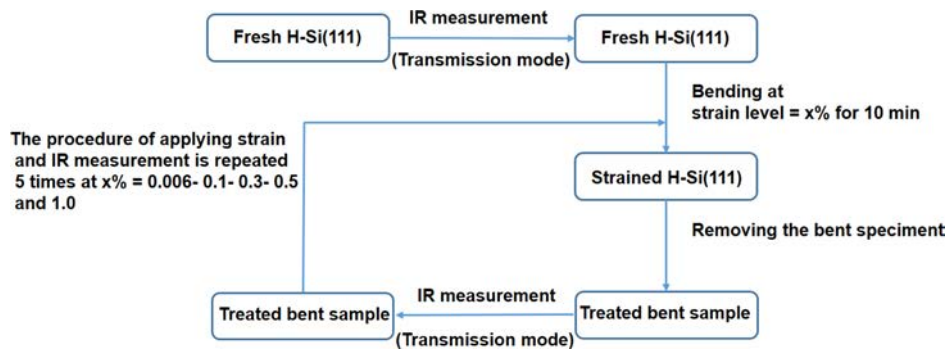


Figure 2. Flow diagram of applying strain and measuring the IR spectra of hydrogen terminated Si(111).

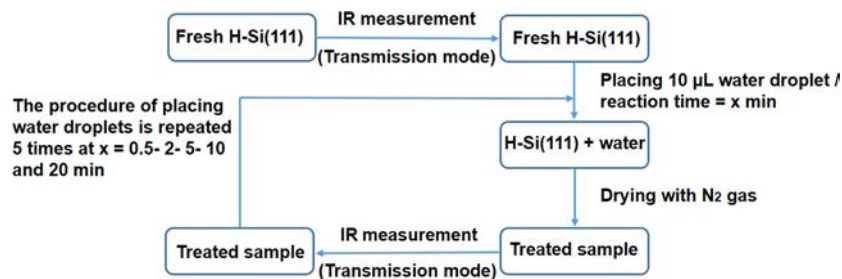


Figure 3. Flow diagram of the procedure to study the reactivity of unstrained hydrogen terminated silicon toward liquid water at different reaction times of 0.5, 2, 5, 10, and 20 min.

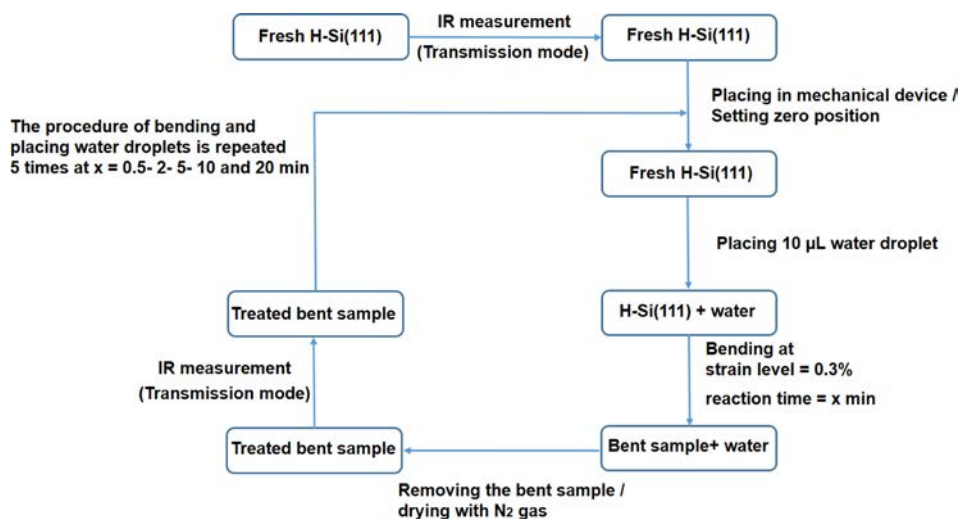


Figure 4. Flow diagram of the procedure to study the reactivity of strained hydrogen terminated silicon (strain level = 0.3%) toward liquid water at different reaction times of 0.5, 2, 5, 10, and 20 min.

in transmission mode is measured. In the next step, after completing the IR measurement, again the sample is placed inside the sample holder, which goes to the zero position. At this time, the spindle completes 5000 steps, which correspond to a strain of the sample of 0.1%. After retaining under stress for 10 min, the bent specimen is removed and the third IR spectrum is measured afterward. This procedure continues until reaching a strain value of 1.0%. All the absorbance spectra are processed by subtracting the IR spectrum of the sample after piranha cleaning and then by flattening the baseline to remove drifts. OPUS software was used to integrate the peak areas, and, when appropriate, peaks were fitted using Origin software. The flow diagram of steps and procedures of this experiment is shown in Figure 2.

At stage (II), the first IR spectrum of fresh H-Si(111) is measured and the side of the sample, which has been in front of the IR beam, is marked. Next, using the calibrated micropipette (10–100 μ L/Eppendorf), 10 μ L deionized water (resistivity 18.2 M Ω cm) is placed at the center of the sample (on the marked side). After 0.5 min of the reaction time, the sample is completely dried using N₂ gas, and the second IR spectrum is measured. Following the IR measurement, the same volume of water is placed on the sample again. The sample is dried after 2 min of reaction time and the third IR spectrum is taken. The same procedure is repeated for the reaction times of 5, 10, and 20 min as well. Figure 3 represents the procedure of experiment.

To accomplish stage (III), the strain value is kept constant at 0.3% and the experiment is performed at different reaction

times. The IR spectrum of fresh H–Si(111) is measured, and the side of the sample that was in front of the IR beam is marked. The sample is placed in the machine (marked side up). First, it reaches the zero position and using the calibrated micropipet (10–100 μL /Eppendorf), 10 μL deionized water (a resistivity of 18.2 $\text{M}\Omega\text{ cm}$) from the same container (a quartz beaker with a quartz cap) that we stored in the glovebox for the experiment (II) is placed at the center of the sample (on the marked side). Then, it is bent following 123 μm downward movement of sample holder (strain level = 0.3%). After 0.5 min of reaction time, the bent sample is removed and is completely dried by N_2 gas. The second IR measurement is performed in the transmission mode. After IR measurement, the sample is placed in the machine, which goes to the zero position. The same volume of deionized water is placed at the center of the sample and strained by applying 0.3% strain. After 2 min of reaction time, the curvature is removed, the sample gets dried, and the sample is made ready for IR measurement. This procedure is repeated 5 times as well by changing the reaction time of bent H–Si(111) toward liquid water (Figure 4).

2.3. Computational Details. DFT calculations were performed as implemented in the Vienna ab initio simulation package (VASP)^{27,28} using the Perdew–Burke–Ernzerhof (PBE) generalized gradient approximation exchange–correlation functional.²⁹ The electron–ion interaction is described by the projector augmented wave (PAW) method³⁰ with an energy cutoff of 360 eV. A super cell with 72 (Si: 54 and H: 18) atoms was completely relaxed for all of the samples studied, with geometry optimization using the conjugate gradient method. Periodic boundary conditions were applied in all directions. The Brillouin zone was sampled using a $4 \times 4 \times 1$ k point mesh size with a Monkhorst–Pack mesh.³¹ Uniaxial loading conditions were applied after the optimized structure was obtained. To apply strain using the uniaxial tensile simulations, we elongated the periodic simulation box size along the loading direction [100] in one step with an engineering strain of 0.3%. The strain value is aligned with the experimentally obtained strain values (strain range 0.006–1.0%). The applied elongation, ΔL , can be obtained based on the initial length of the unstrained sample along the loading direction, L_0 , and the loading engineering strain, which is equivalent to $\Delta L/L_0$. The simulation box size in the perpendicular direction of the loading was then adjusted accordingly to ensure uniaxial stress conditions in the study, so that stress remained negligible in the perpendicular direction.³² After applying the loading conditions, structural relaxation was achieved using the conjugate gradient energy minimization method with 10^{-6} eV criteria for energy convergence. To calculate the IR spectra, the IBIRON = 8 is set to determine the Hessian matrix (matrix of second derivatives).

Kinetic barriers were calculated by the nudged elastic band (NEB) method, using a string of geometric configurations to describe the reaction pathway of the system. A spring interaction between every configuration ensured continuity of the reaction pathway.

3. RESULTS AND DISCUSSION

3.1. Strain Effect on the Microstructure of H–Si(111).

Figure 5 demonstrates the IR spectra of H–Si(111) obtained after the mechanical test of the sample. The presence of a Si–H stretching peak (2083.3 cm^{-1}) for the surface is confirmed by the Si–H stretching vibration.^{17,33} The dark blue curve

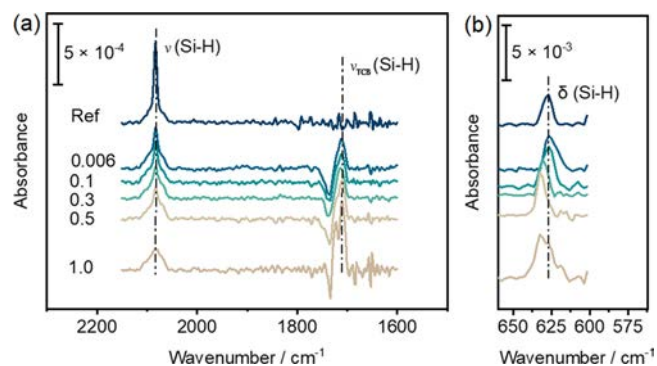


Figure 5. FTIR spectra of the H–Si(111) surface subjected to different strain levels (percent). The dark blue spectrum (Ref) corresponds to the unstrained sample (fresh H–Si(111)). Spectrum of sample (Si(111)) obtained after piranha cleaning is used as the background for all the presented spectra.

(Ref) shows the IR spectrum of fresh H–Si(111) before bending. The peak intensity in the stretching Si–H mode is decreased by 54.2% following exposure of strain of 0.006% for 10 min. After strain enhancement to 0.3%, the intensity of the Si–H peak reaches a value that is 64.2% less than that of the unstrained sample (dark blue curve). At higher strain, the decreasing trend becomes slower and at the 1.0% strain, the intensity decreases substantially to about 1/3 of the initial intensity. Deconvolution of absorbance bands into an elementary contribution is carried out using Origin software. The spectra are fitted by the Lorentz profile and the data for the best fit are presented in Supporting Information.

Following strain enhancement (Figure 6a), a decrease in the intensity of Si–H stretching mode (at 2083.3 cm^{-1}) possibly means a decrease of the total bonded hydrogen. However, increasing the strain causes the amplitude of the band at 626.40 cm^{-1} to fluctuate in peak intensity (Figure 6c). Altogether, it is suggested that redistribution of the bonded hydrogen in the silicon network happened during the bending rather than decreasing in the hydrogen content.³⁴ Furthermore, strained samples develop a band at $\sim 1712\text{ cm}^{-1}$, which becomes sharper upon strain elevation (Figures 5a and 6b). There is no peak of the IR spectrum (Figure 5a) at 1712 cm^{-1} for the unstrained sample (dark blue curve).

Dissociation and transformation of some hydrogen bonding configurations into other configurations may be the underlying reason for stretching band intensity.³⁴ In the current case, the appearance of a new band in the vibrational spectra of the bonded hydrogen is anticipated. Because experiments (applying strain and measuring the IR spectra) are performed inside a N_2 purged glovebox, the potential source of contamination is not involved in the band at $\sim 1712\text{ cm}^{-1}$. We hypothesize that the generation of a new band is due to the intensity change in the bending mode at 626.40 cm^{-1} . Furthermore, deconvolution of the Si–H bending mode (626.40 cm^{-1}) into three components (see Supporting Information, Figure S3) led to the discovery of even more new bending modes.

The redistribution of hydrogen during the bending is clearly demonstrated in Figure 6, where we display the intensity of the bending band (626.40 cm^{-1}) and the intensity of the band at 2083.3 cm^{-1} as a function of strain. A decrease in intensity of the stretching band and a fluctuation in intensity of the bending band occur with the appearance of a new peak at $\sim 1712\text{ cm}^{-1}$. Diffusion of a hydrogen atom from the Si–H site

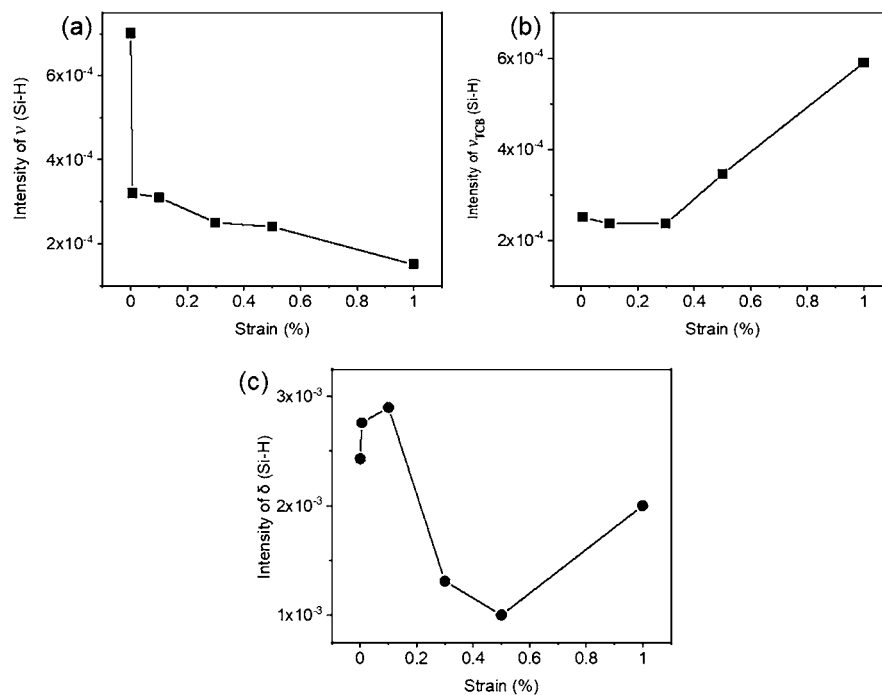


Figure 6. Variation of peak intensity as a function of strain: (a) intensity of the stretching Si–H mode, (b) intensity of the newly induced band (three center bond (TCB)) due to the strain effect, and (c) intensity of the bending Si–H mode. All of the peaks are fitted by the Lorentzian function (Supporting Information, Tables S1, S2, and S4).

to form a three center bond (TCB): Si–H–Si could be a reason.³⁴ The formation of a TCB in crystalline silicon is predicted in which two silicon atoms harbor the hydrogen atom (bond centered hydrogen) or in an asymmetric position.^{35–37} The hydrogen is bonded to silicon atoms occupying the antibonding (AB) positions in hydrogenated n type GaAs: Si, and there is a line corresponding to the Si–H vibration at 1717 cm^{-1} .³⁸ Several infrared transmission spectra show that hydrogen is capable of occupying two kinds of sites in hydrogenated amorphous boron (a B–H), a bridging hydrogen site (three B–H–B bond) or a terminal site (B–H).³⁹ The B–H complex and B–H–B show their absorption band at 2560 and 2050 cm^{-1} , respectively. Findings that resonate from the above discussion are as follows: (a) a stretching band at frequency very similar to those of the corresponding complexes as in crystalline or amorphous silicon is observed in the Si–H modes of strained H–Si(111); and (b) the Si–H bond with H in the TCB position is detected in our sample at a frequency that is lower than the stretching mode at 2038.3 cm^{-1} . According to the analogy of Si–H in H–Si(111) and B–H in a B:H or other similar examples, the band in strained H–Si(111) at $\sim 1712 \text{ cm}^{-1}$ is proposed to be attributed to the stretching mode of TCB Si–H–Si formed during bending. The current findings are easily interpreted using the hydrogen diffusion model if the mentioned assignment is correct.

Dissociation of Si–H bonds next to weak Si–Si bonds occurs when strain along the [100] direction is applied. In this regard, the H atom traverses to the off bond sites leading to termination of a normal dangling bond.³⁴ Relying on this background, a new model for ϵ H–Si(111) with a Si–H–Si bond is constructed. The atomic configuration of the relaxed unstrained and strained models is shown in Figure 7a.

The strained model (Figure 7a) is constructed in which strain is applied in the direction of [100] with orientation of

metastable Si–H–Si bonds in relation to the directions of Si–Si back bonds; the [441] direction. As is shown,¹⁵ the reactivity of the bonds is increased by the strain, especially in those most nearly aligned with the direction of the stress. Because the [441] direction has a lower angle ($\theta = 35.1^\circ$) with the strain direction (Supporting Information, Figure 4), the oriented bonds in this direction are more affected, and the probability of Si–H–Si formation is higher along [441].

According to the calculations, a new orientation on the surface is evident by the hydrogen because of the strain. This demonstrates the ability of hydrogen to relieve strain on the network.¹ In Table 2, data of changes in the bond length of the Si–Si back bonds and Si–H following strain are shown. In this model, as the optimized structure indicates H is not located at the center between two host Si atoms, the optimized Si–H distance becomes 1.77 and 1.53 \AA with a Si–H–Si angle of 121.6° (Figure 7d). Importantly, the experimental findings and the assumptions of the TCB model are in accordance with the results obtained using DFT calculations of the relevant vibrational frequencies. The calculated IR spectra of unstrained H–Si(111) and strained models are demonstrated in Figure 7e. The experimental results confirmed the presence of a new Si–H stretching mode at around 1915 cm^{-1} and remarkable alterations in the intensity of Si–H stretching and bending modes. Therefore, the calculated peak at 1915 cm^{-1} corresponds to the measured peak at 1712 cm^{-1} . To interpret the observed new peak, we used Molden,⁴⁰ a visualization tool that allowed us to assign the calculated vibrational modes as accurately as possible (Supporting Information, Table S3). Activation energy for the production of the metastable Si–H–Si configuration is significantly high, around 1.5 eV .⁴¹ However, this activation energy would be 1.7 eV based on our calculations.⁴¹ The Si–Si bond next to the Si–H bond is weakened because the electronegativity of H is higher compared with that of Si. The H atoms possibly hop back to

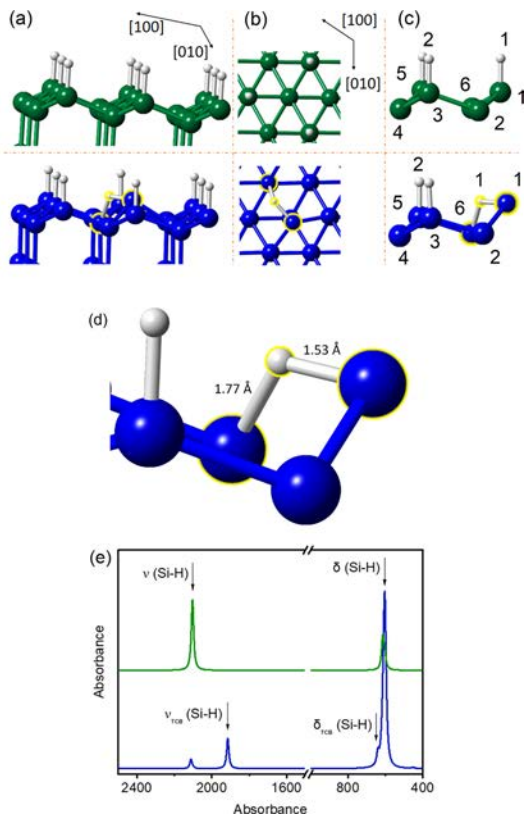


Figure 7. Possible configuration that resulted from the strain effect on Si-Si and Si-H bond length and orientation; hydrogen diffusion, breaking of the Si-Si bond, and formation of Si-H-Si (TCB). (a,b) Side and top views of models, respectively. (c) Part of models that experienced a higher change following hydrogen movement. Information regarding the Si-Si and Si-H bonds (presented in (c)) is provided in Table 2. (d) Measured bond distance of Si-H-Si using CrystalMaker software, and (e) calculated IR spectra of unstrained H-Si(111) (green curve) and 0.3% strained model (along [100] direction) containing the Si-H-Si bond (blue curve). Molden is used to define the type of the vibrational modes of the TCB (Supporting Information, Table S3).

Table 2. Calculated Si-Si and Si-H Bond Lengths for the Optimized Structures of Two Models, Unstrained H-Si(111) and Strained H-Si(111)

bond length/Å	unstrained H Si(111)	strained H Si(111)
Si ₁ H ₁	1.504	1.531
Si ₅ H ₂	1.504	1.054
Si ₁ Si ₂	2.343	2.373
Si ₂ Si ₃	2.343	2.352
Si ₃ Si ₄	2.343	2.350
Si ₄ Si ₅	3.343	2.345
Si ₅ Si ₆	3.343	2.350
Si ₆ Si ₁	3.343	2.890
Si ₆ H ₁	1.504	1.776

their initial configuration or diffuse apart upon the formation of Si-H-Si sites.⁴¹ A larger length of the Si-H bond in the three center configuration than in its initial configuration (Si-H/1.5 Å) makes the bond of the H atom loose (metastable).

The calculated IR spectrum (blue curve, Figure 7e) also shows the splitting of the bending Si-H mode. The vibrational mode of a new peak (at 640.46 cm⁻¹), which shows the bending vibration related to TCB, is assigned using the

Molden software. This observation aids in the identification of different species obtained by deconvolution of the measured bending Si-H peak in the experiment (Figure 5b). We concluded that the splitting of the bending mode into three components may arise from (1) the formation of TCBs [frequency higher than ~626.40 cm⁻¹ (terrace monohydride bending mode) for the strained samples] and (2) in agreement with refs 42 and 43, we attribute the bending mode measured at a lower frequency than 626.40 cm⁻¹ to monohydride step vibrations.

3.2. Surface Reactivity of Unstrained H-Si(111) toward Liquid Water. The chemical stability of a passivated Si substrate is determined by two forms of bonds: up Si-H bonds and Si-Si back bonds to the underlying layer. In order to have a better understanding as well as controlling of the chemical processes on H terminated silicon surfaces, there is an essential need to characterize the chemical reactivity of these bonds. As a result, in this study, the reactivity of up Si-H bonds is investigated first, followed by the reactivity of Si-Si back bonds.

The IR spectra of H-Si(111) samples before and after reaction with water at various reaction times are shown in Figure 8. Monohydride Si gives rise to one peak at 2083.7 cm⁻¹ after treatment of the surface with HF/NH₄F.¹⁷ The IR spectrum of fresh H-Si(111) before reactivity with water is shown in the black curve (Ref). When the surface is reacted with water at different reaction times (green IR spectra), the Si-H peak almost remains unchanged. As previously shown in the experimental observations, the reaction between water vapor and the H-Si(111) surface occurs at a temperature threshold of 350 °C in which the OH dipole replaces with adsorbed H.⁴⁴ It implies that there is an energy barrier that must be resolved in order for the reaction to begin. NEB calculations are used to obtain more details about the reaction pathway and energy barriers. The relevant energy profile for oxidation of Si-H and Si-Si back bonds along the reaction pathway is depicted in Figure 8c. The activation energy of 1.8 eV (41.5 kcal mol⁻¹) characterizes the H₂O reaction with Si-H site on the flat surface forming Si-OH and H₂ (g) (Figure 8c, panel b). The reaction is exothermic with a ΔE value of -0.5 eV (-11.5 kcal mol⁻¹). As a result, the oxidation of up Si-H bonds (Si-H → Si-OH) is hindered by a high energy barrier of 1.8 eV.

Peaks in the range of 2100–2300 and 1000–1250 cm⁻¹ relating to the oxide surface, O_x SiH and SiO_x, respectively, are predicted to be observed during the oxidation of Si-Si back bonds.¹⁷ No peak in the IR spectra can be found in the described ranges, as shown in Figure 8a,b (green curves). Therefore, we proceed our NEB calculations to determine the energy barriers for the oxidation of Si-Si back bonds. According to calculations (Figure 8c, panel c), the insertion of the OH group of Si-OH into the Si-Si back bond is hampered by high energy 3.2 eV (73.79 kcal mol⁻¹). However, transferring the H atom of OH toward the close silyl radical (panel d) encounters a barrier of 0.84 eV (19.37 kcal mol⁻¹). Consequently, achieving the oxidized surface from a surface containing Si-OH group needs to overcome the high energy barriers. Incorporating very high temperature to the system is a way to address the highly important issue.^{17,44} The absence of a peak corresponding to the oxidation of the silicon surface may be due to the existence of high energy barriers for the last steps (Figure 8c).

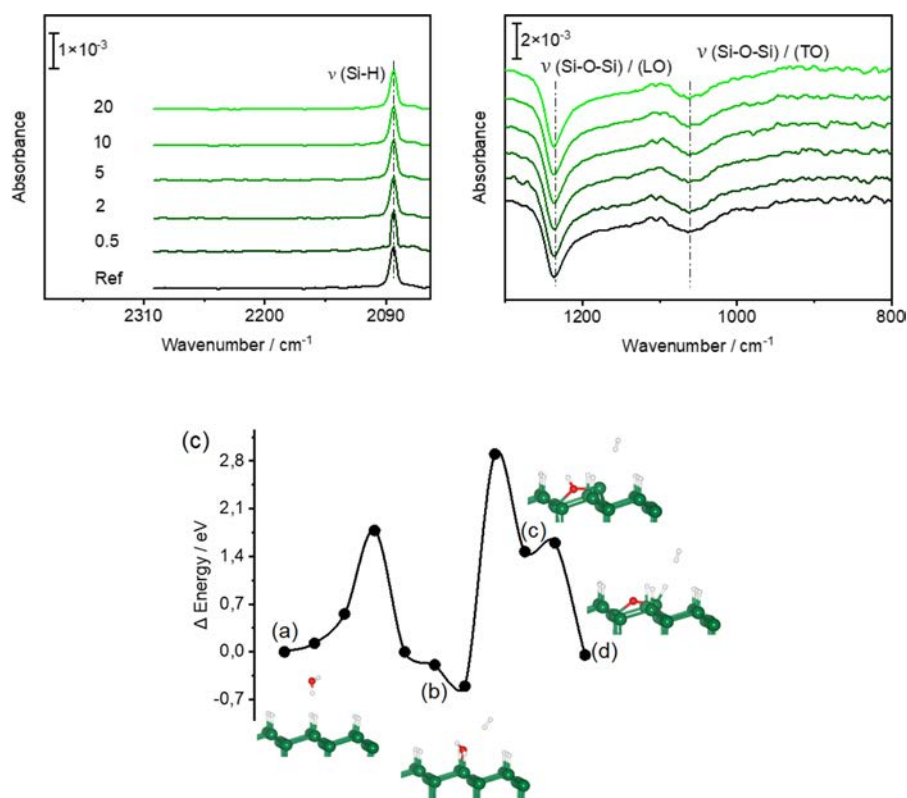


Figure 8. FTIR spectra of an unstrained H-Si(111) before (black curve, Ref) and after reaction with water (green curves) as a function of reaction time. The numbers (0.5, 2, 5, 10, and 20) represent the reaction times, which are expressed in minute. The spectrum of the sample after piranha cleaning (not shown) is used as the background for all spectra. For clarity, the results are plotted into separate spectra regions of (a) 2310–2050 and (b) 1300–800 cm^{-1} . (c) Energy profile as a function of reaction coordinate for the reaction of water with the Si-H bond and the Si-Si back bond. The panels (a–d) indicate the energy of the critical points taking as a reference the water molecule adsorbed on the surface.

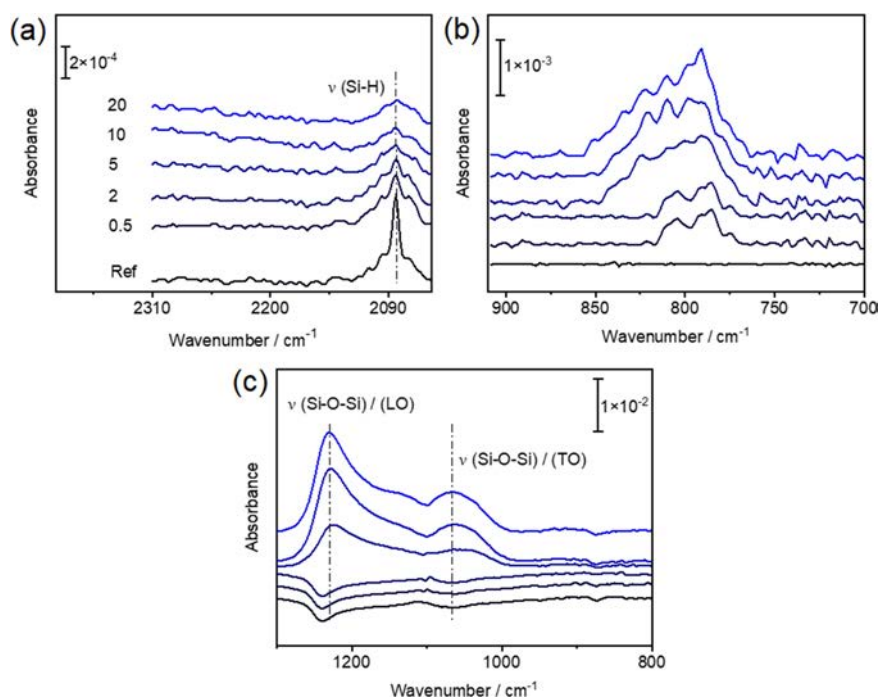


Figure 9. FTIR spectra of strained H-Si(111) after reaction with water as a function of reaction time. Black curve (Ref) is the spectrum of the fresh $\text{NH}_4\text{F}/\text{HF}$ treated sample. The absorbance spectra are processed by subtracting the IR spectrum of the sample after piranha cleaning. The numbers (0.5, 2, 5, 10, and 20) show the reaction times (expressed in minute) of strained H-Si(111) (strain = 0.3%) with water. The spectra are separated into three important regions; (a) Si-H stretching peak, (b) generation of the bending Si-OH mode, and (c) the formation of Si-O-Si phonon modes. The data for the best fit with Lorentzian function are provided in Supporting Information, Figures S5–S7.

3.3. Surface Reactivity of Strained H–Si(111) toward Liquid Water. As in Section 3.2, the reactivity of up Si–H bonds is studied first, followed by the reactivity of Si–Si back bonds.

The FTIR spectrum of fresh H–Si(111) is displayed in Figure 9 (black curve, Ref). The IR spectra of a strained H–Si(111) (strain = 0.3%) after reaction with water are shown in blue curves as a function of reaction time. After 0.5 min of water reaction with the strained surface, the intensity of the Si–H stretching mode decreases (Figure 9a). This suggests oxidation of up Si–H bonds (replacing the H with OH groups). It is important to note that oxidation of up bonds is not the only factor that can cause the Si–H band intensity to decline. Because the IR spectra of the sample after piranha cleaning is used as a background for all spectra, the effect of strain on decreasing Si–H stretching band intensity should also be considered (as explained in the Section 3.1).

The appearance of the Si–OH bending mode (800–1000 cm^{-1}) could possibly confirm the substitution of some atop Si–H groups with atop OH groups.^{45–47} The peak related to the bending mode for Si–OH groups is around 809.61 cm^{-1} (Figure 9b), [see Supporting Information (Figure S5 and Table S5)]. As a result, in comparison to unstrained H–Si(111), the results show that after reactivity with water, up Si–H bonds in ϵ H–Si(111) are oxidized. The oxidation of up Si–H bonds in ϵ H–Si(111) is also confirmed by our DFT calculations (Supporting Information, Figure S9).

Positive absorption modes at ~ 1050 and ~ 1220 cm^{-1} in Figure 9c, which are sequentially associated with the asymmetric Si–O–Si transverse optical and Si–O–Si longitudinal optical stretching modes, show oxidation of the silicon surface.^{8,9,45} Remarkably, there is no Si–O–Si oxidation species underneath surface bound Si–H sites as no clear absorption appeared in the range of 2150–2300 cm^{-1} (Figure 9a), which represents Si–H species with oxygen inserted in the Si–Si back bonds (designated as O_x SiH species).^{17,48} The O_x SiH modes are absent in this study as compared to experiments on H–Si(111) samples under certain conditions such as gas phase O_2 or H_2O at high temperatures.¹⁷ These results suggest the dominance of different oxidation pathways while strain is applied to the samples.

After 0.5 and 2 min of reaction, the Si–H stretching modes are reduced, accompanied by rapid generation of Si–O–Si peaks and continuous Si–OH intensity enhancement. Two important points could be extracted from Figure 9: the formation of oxide was retarded in spite of a decrease in Si–H intensity during the first 2 min of reaction time; the oxide thickness did not commence to increase concurrently as the Si–H intensity decreases. This provides the proof that the reduction in Si–H intensity only resulted from the strain effect and oxidation of up Si–H bonds. The surface is attacked easily by H_2O when oxidation (partially) occurs at the topmost layer of the H–Si(111) surface resulting in a sharp increase in the Si–O stretching vibration. It seems that Si–OH groups might remain intact throughout the oxidation of back bonds substantiating a continuous increase in Si–OH.

Two possibilities are proposed for rapid surface oxidation; formation of (1) $\text{O}_x\text{Si OH}$ or (2) SiO_x . Any shift in the Si–OH vibration mode could be seen upon residing of the oxygen atoms directly beneath the Si–OH.⁴⁵ The obtained peak frequency related to the Si–OH mode for different reaction times of the surface with water (Supporting Information, Table S5) shows that the frequency almost remained unchanged

around 809.61 cm^{-1} . DFT calculations are carried out on three Si–OH terminated ϵ H–Si(111) surfaces in order to test this hypothesis (Supporting Information, Figure S8). The concluding remark could be the surface was covered by $\text{Si}_3\text{Si–OH}$ and SiO_x groups. The surface oxidation of hydroxylated H–Si(111) with water is investigated using NEB calculations to support these results.

The initial structure we use is hydroxylated ϵ H–Si(111), which is strained along [100] and contains the Si–H–Si group along the [441] direction. According to the NEB calculations, this reaction progresses through two low energy barriers [E value = -0.481 eV (-11.09 kcal mol^{-1})] (Figure 10). A H_2

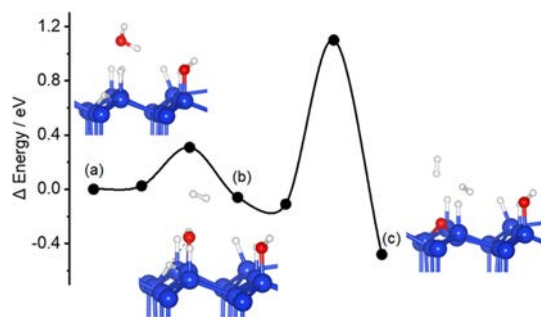


Figure 10. Energy profile for the reaction of hydroxylated strained H–Si(111) with water. (a–c) Initial, intermediate, and final structures, respectively.

species and an OH group (panel b) are produced following the reaction between water and the metastable Si–H–Si bond with a ΔE value of 0.3 eV (6.9 kcal mol^{-1}). Then, conversion into Si–O–Si bonds, as shown in panel c, with an activation energy of 1.0 eV (23 kcal mol^{-1}), occurred. The final remark may be the $\text{Si}_3\text{Si–OH}$ and SiO_x groups cover the surface of strained H–Si(111) after the reaction with liquid water.

4. CONCLUSIONS

Two types of bonds, the up Si–H bonds and the Si–Si back bonds to the underlying layer, determine the chemical stability of a passivated Si substrate. In order to have a better understanding as well as controlling of the chemical processes on H terminated silicon surfaces, there is an essential need to characterize the chemical reactivity of the bonds. The dominant chemical process under an ambient condition is oxidation. The rate of oxidation is influenced by environmental factors, the presence of reacting agents, and inherent sample specifications such as surface morphology. The spectra presented in this work demonstrate prominent aspects of the chemistry of the silicon surface, which is affected by strain. First, strain shows its potential to change the pathway of the reaction of the hydrogen terminated surface that considerably shifts the kinetics of surface reactions. There is high priority of oxidation in subsurface Si–Si back bonds only after 5 min of the reaction time. This finding underlines the catalyzing role of strain in surface reactivity to overcome the activation energies. This study also revealed that Si–OH linkages with substrate oxidation are produced upon the reaction between water and the strained hydrogen terminated surface. Also, it demonstrates the existence of oxidants producing the oxide layer; hydrated silicon oxide (Si–OH) and SiO_x species. We concluded in this study that strain causes fast oxidation of the Si–Si backbone, and Fuchs et al.⁴⁹ demonstrated that oxygen atoms incorporated directly into Si–Si bonds at the

interface are a source of optical anisotropy and induce strain on the structure. As a result, it is also worth noting that applied strain on the structure and Si–Si back bond oxidations are mutually exclusive.

AUTHOR INFORMATION

Corresponding Author

Peter Thissen – Karlsruhe Institute of Technology, Institute of Functional Interfaces, 76344 Eggenstein Leopoldshafen, Germany; [orcid.org/0000 0001 7072 4109](https://orcid.org/0000-0001-7072-4109);
Email: peter.thissen@kit.edu

Authors

Tahereh Mohammadi Hafshejani – Karlsruhe Institute of Technology, Institute of Functional Interfaces, 76344 Eggenstein Leopoldshafen, Germany

Jonas Wohlgemuth – Karlsruhe Institute of Technology, Institute of Functional Interfaces, 76344 Eggenstein Leopoldshafen, Germany

Notes

The authors declare no competing financial interest.

ACKNOWLEDGMENTS

This work was supported by the DFG funded project TH 1566/6–1.

REFERENCES

- (1) Tuttle, B.; Van de Walle, C. G. Structure, energetics, and vibrational properties of Si H bond dissociation in silicon. *Phys. Rev. B: Condens. Matter Mater. Phys.* **1999**, *59*, 12884.
- (2) Pankove, J. I.; Johnson, N. M. *Hydrogen in Semiconductors: Hydrogen in Silicon*; Academic Press, 1991.
- (3) Gokce, B.; Aspnes, D. E.; Lucovsky, G.; Gundogdu, K. Bond specific reaction kinetics during the oxidation of (111) Si: Effect of n type doping. *Appl. Phys. Lett.* **2011**, *98*, 021904.
- (4) Mizsei, J. Fermi level pinning and passivation on the oxide covered and bare silicon surfaces and interfaces. *Vacuum* **2002**, *67*, 59–67.
- (5) Soria, F. A.; Patrino, E. M.; Paredes Olivera, P. Oxidation of hydrogenated Si (111) by a radical propagation mechanism. *J. Phys. Chem. C* **2012**, *116*, 24607–24615.
- (6) Chabal, Y. J.; Feldman, L. C. Silicon surface and interface issues for nanoelectronics. *Electrochem. Soc. Interface* **2005**, *14*, 31–33.
- (7) Muller, D. A.; Sorsch, T.; Moccio, S.; Baumann, F. H.; Evans Lutterodt, K.; Timp, G. The electronic structure at the atomic scale of ultrathin gate oxides. *Nature* **1999**, *399*, 758–761.
- (8) Queaney, K. T.; Herbots, N.; Shaw, J. M.; Atluri, V.; Chabal, Y. J. Infrared spectroscopic analysis of an ordered Si/SiO₂ interface. *Appl. Phys. Lett.* **2004**, *84*, 493–495.
- (9) Weldon, M. K.; Queaney, K. T.; Chabal, Y. J.; Stefanov, B. B.; Raghavachari, K. Mechanistic studies of silicon oxidation. *J. Vac. Sci. Technol., B: Microelectron. Nanometer Struct. Process., Meas., Phenom.* **1999**, *17*, 1795–1802.
- (10) Juarez, M. F.; Soria, F. A.; Patrino, E. M.; Paredes Olivera, P. Influence of subsurface oxidation on the structure, stability, and reactivity of grafted Si (111) surfaces. *J. Phys. Chem. C* **2008**, *112*, 14867–14877.
- (11) Irene, E. Applications of spectroscopic ellipsometry to microelectronics. *Thin Solid Films* **1993**, *233*, 96–111.
- (12) Gibson, J. M.; Lanzerotti, M. Y. Observation of interfacial atomic steps during silicon oxidation. *Nature* **1989**, *340*, 128–131.
- (13) Tsai, V.; Wang, X. S.; Williams, E. D.; Schneir, J.; Dixon, R. Conformal oxides on Si surfaces. *Appl. Phys. Lett.* **1997**, *71*, 1495–1497.
- (14) Yen, J. Y.; Hwu, J. G. Enhancement of silicon oxidation rate due to tensile mechanical stress. *Appl. Phys. Lett.* **2000**, *76*, 1834–1835.
- (15) Gokce, B.; Adles, E. J.; Aspnes, D. E.; Gundogdu, K. Measurement and control of in plane surface chemistry during the oxidation of H terminated (111) Si. *Proc. Natl. Acad. Sci. U.S.A.* **2010**, *107*, 17503–17508.
- (16) Bergfeld, S.; Braunschweig, B.; Daum, W. Nonlinear optical spectroscopy of suboxides at oxidized Si (111) interfaces. *Phys. Rev. Lett.* **2004**, *93*, 097402.
- (17) Zhang, X.; Chabal, Y. J.; Christman, S. B.; Chaban, E. E.; Garfunkel, E. Oxidation of H covered flat and vicinal Si (111) 1 × 1 surfaces. *J. Vac. Sci. Technol., A* **2001**, *19*, 1725–1729.
- (18) Juarez, M. F.; Patrino, E. M.; Paredes Olivera, P. Quantum Mechanical Investigation of the Influence of the Local Environment on the Vibrational Properties of Hydrogenated Si (111). *J. Phys. Chem. C* **2009**, *113*, 681–690.
- (19) Michalak, D. J.; Rivillon, S.; Chabal, Y. J.; Estève, A.; Lewis, N. S. Infrared spectroscopic investigation of the reaction of hydrogen terminated, (111) oriented, silicon surfaces with liquid methanol. *J. Phys. Chem. B* **2006**, *110*, 20426–20434.
- (20) Chen, L.; He, X.; Liu, H.; Qian, L.; Kim, S. H. Water adsorption on hydrophilic and hydrophobic surfaces of silicon. *J. Phys. Chem. C* **2018**, *122*, 11385–11391.
- (21) Israelachvili, J.; Wennerström, H. Role of hydration and water structure in biological and colloidal interactions. *Nature* **1996**, *379*, 219–225.
- (22) Klein, J. Repair or replacement: a joint perspective. *Science* **2009**, *323*, 47–48.
- (23) Ben Naim, A. Y. *Hydrophobic interactions*; Springer Science & Business Media, 2012.
- (24) Raschke, T. M. Water structure and interactions with protein surfaces. *Curr. Opin. Struct. Biol.* **2006**, *16*, 152–159.
- (25) Jaccodine, R. J. Surface Energy Of Germanium And Silicon. *J. Electrochem. Soc.* **1963**, *110*, 524–527.
- (26) Hafshejani, T. M.; Feng, C.; Wohlgemuth, J.; Krause, F.; Bogner, A.; Dehn, F.; Thissen, P. Effect of polymer coated silica particles in a Portland cement matrix via in situ infrared spectroscopy. *J. Compos. Mater.* **2021**, *55*, 475.
- (27) Kresse, G.; Furthmüller, J. Efficiency of ab initio total energy calculations for metals and semiconductors using a plane wave basis set. *Comput. Mater. Sci.* **1996**, *6*, 15–50.
- (28) Kresse, G.; Furthmüller, J. Efficient iterative schemes for ab initio total energy calculations using a plane wave basis set. *Phys. Rev. B: Condens. Matter Mater. Phys.* **1996**, *54*, 11169.
- (29) Perdew, J. P.; Burke, K.; Ernzerhof, M. Generalized gradient approximation made simple. *Phys. Rev. Lett.* **1996**, *77*, 3865.
- (30) Kresse, G.; Joubert, D. From ultrasoft pseudopotentials to the projector augmented wave method. *Phys. Rev. B: Condens. Matter Mater. Phys.* **1999**, *59*, 1758.
- (31) Chadi, D. J.; Cohen, M. L. Special points in the Brillouin zone. *Phys. Rev. B: Solid State* **1973**, *8*, 5747.
- (32) Mortazavi, B.; Rahaman, O.; Dianat, A.; Rabczuk, T. Mechanical responses of borophene sheets: a first principles study. *Phys. Chem. Chem. Phys.* **2016**, *18*, 27405–27413.
- (33) Miura, T. a.; Niwano, M.; Shoji, D.; Miyamoto, N. Initial stages of oxidation of hydrogen terminated Si surface stored in air. *Appl. Surf. Sci.* **1996**, *100–101*, 454–459.
- (34) Darwich, R.; Cabarrocas, P. R. I.; Vallon, S.; Ossikovski, R.; Morin, P.; Zellama, K. Observation by infrared transmission

spectroscopy and infrared ellipsometry of a new hydrogen bond during light soaking of a Si: H. *Philos. Mag. B* **1995**, *72*, 363–372.

(35) Estreicher, S. Equilibrium sites and electronic structure of interstitial hydrogen in Si. *Phys. Rev. B: Condens. Matter Mater. Phys.* **1987**, *36*, 9122.

(36) Deák, P.; Snyder, L. C.; Corbett, J. W. State and motion of hydrogen in crystalline silicon. *Phys. Rev. B: Condens. Matter Mater. Phys.* **1988**, *37*, 6887.

(37) Van de Walle, C. G. Energies of various configurations of hydrogen in silicon. *Phys. Rev. B: Condens. Matter Mater. Phys.* **1994**, *49*, 4579.

(38) Pajot, B.; Clerjaud, B.; Chevallier, J. Vibrational properties of hydrogen in compound semiconductors. *Phys. B* **1991**, *170*, 371–382.

(39) Godet, C.; Schmirgeld, L.; Zuppiroli, L.; Sardin, G.; Gujrathi, S.; Oxorn, K. Optical properties and chemical reactivity of hydrogenated amorphous boron thin films. *J. Mater. Sci.* **1991**, *26*, 6408–6418.

(40) Schaftenaar, G.; Noordik, J. H. Molden: a pre and post processing program for molecular and electronic structures. *J. Comput. Aided Mol. Des.* **2000**, *14*, 123–134.

(41) Godet, C.; Roca i Cabarrocas, P. Role of Si–H bonding in a Si: H metastability. *J. Appl. Phys.* **1996**, *80*, 97–102.

(42) Caudano, Y.; Thiry, P. A.; Chabal, Y. J. Investigation of the bending vibrations of vicinal H/Si (111) surfaces by infrared spectroscopy. *Surf. Sci.* **2002**, *502–503*, 91–95.

(43) Watanabe, S.; Sugita, Y. Anisotropic dynamic polarization of surface vibrations associated with H on stepped Si (111). *Chem. Phys. Lett.* **1995**, *244*, 105–110.

(44) Zaïbi, M. A.; Sébenne, C. A.; Lacharme, J. P. Temperature Activated Reactions of H₂O and NH₃ with H Passivated Si (111) Surfaces. *Surf. Rev. Lett.* **2001**, *08*, 25–31.

(45) Michalak, D. J.; Amy, S. R.; Estève, A.; Chabal, Y. J. Investigation of the chemical purity of silicon surfaces reacted with liquid methanol. *J. Phys. Chem. C* **2008**, *112*, 11907–11919.

(46) Thissen, P.; Peixoto, T.; Longo, R. C.; Peng, W.; Schmidt, W. G.; Cho, K.; Chabal, Y. J. Activation of surface hydroxyl groups by modification of H terminated Si (111) surfaces. *J. Am. Chem. Soc.* **2012**, *134*, 8869–8874.

(47) Iftiquar, S. Structural studies on semiconducting hydrogenated amorphous silicon oxide films. *High Temp. Mater. Processes* **2002**, *6*, 19.

(48) Miura, T. a.; Niwano, M.; Shoji, D.; Miyamoto, N. Kinetics of oxidation on hydrogen terminated Si (100) and (111) surfaces stored in air. *J. Appl. Phys.* **1996**, *79*, 4373–4380.

(49) Fuchs, F.; Schmidt, W.; Bechstedt, F. Understanding the optical anisotropy of oxidized Si (001) surfaces. *Phys. Rev. B: Condens. Matter Mater. Phys.* **2005**, *72*, 075353.

Repository KITopen

Dies ist ein Postprint/begutachtetes Manuskript.

Empfohlene Zitierung:

Hafshejani, T. M.; Wohlgemuth, J.; Thissen, P.
[Strain Activation of Surface Chemistry on H-Terminated Si\(111\)](#)
2021. Journal of Physical Chemistry C
doi: [10.5445/IR/1000138697](https://doi.org/10.5445/IR/1000138697)

Zitierung der Originalveröffentlichung:

Hafshejani, T. M.; Wohlgemuth, J.; Thissen, P.
[Strain Activation of Surface Chemistry on H-Terminated Si\(111\)](#)
2021. Journal of Physical Chemistry C, 125 (36), 19811–19820.
[doi:10.1021/acs.jpcc.1c06309](https://doi.org/10.1021/acs.jpcc.1c06309)

Lizenzinformationen: [KITopen-Lizenz](#)